Peak exclusion, stochasticity and convergence of perturbative bias expansions in 1+1 gravity

Tobias Baldauf, Sandrine Codis, Vincent Desjacques, Christophe Pichon

Monthly Notices
of the
ROYAL ASTRONOMICAL SOCIETY

MNRAS **456,** 3985–4000 (2016) doi:10.1093/mnras/stv2973

Peak exclusion, stochasticity and convergence of perturbative bias expansions in 1+1 gravity

Tobias Baldauf,[1] Sandrine Codis,[2,3]★ Vincent Desjacques[4] and Christophe Pichon[2,5]

[1] *Institute for Advanced Study, School of Natural Sciences, Einstein Drive, Princeton, NJ 08540, USA*
[2] *CNRS, UMR7095 and UPMC Institut d'Astrophysique de Paris, 98 bis Boulevard Arago, F-75014 Paris, France*
[3] *Canadian Institute for Theoretical Astrophysics, University of Toronto, 60 St. George Street, Toronto, ON M5S 3H8, Canada*
[4] *Département de Physique Théorique, Université de Genève, 24, quai Ernest Ansermet. CH-1211, Genève, Switzerland*
[5] *Institute of Astronomy, University of Cambridge, Madingley Road, Cambridge CB3 0HA, UK*

Accepted 2015 December 17. Received 2015 December 17; in original form 2015 October 30

ABSTRACT

The Lagrangian peaks of a 1D cosmological random field representing dark matter are used as a proxy for a catalogue of biased tracers in order to investigate the small-scale exclusion in the two-halo term. The two-point correlation function of peaks of a given height is numerically estimated and analytical approximations that are valid inside the exclusion zone are derived. The resulting power spectrum of these tracers is investigated and shows clear deviations from Poisson noise at low frequencies. On large scales, the convergence of a perturbative bias expansion is discussed. Finally, we go beyond Gaussian statistics for the initial conditions and investigate the subsequent evolution of the two-point clustering of peaks through their Zel'dovich ballistic displacement, to clarify how exclusion effects mix up with scale-dependences induced by non-linear gravitational evolution. While the expected large-scale separation limit is recovered, significant deviations are found in the exclusion zone that tends in particular to be reduced at later times. Even though these findings apply to the clustering of 1D tracers, they provide useful insights into halo exclusion and its impact on the two-halo term.

Key words: methods: analytical – galaxies: statistics – large-scale structure of Universe.

1 INTRODUCTION

Dark matter haloes and the galaxies within them are distinct and extended objects. By definition, they cannot overlap since their centres have to be separated by at least the sum of their virial radii. This exclusion effect is even more important in the initial conditions or Lagrangian space, before the objects collapsed and fell towards each other. As noted in Mo & White (1996) and Sheth & Lemson (1999), the vanishing probability to find two centres closer than the exclusion radius corresponds to the correlation function being -1 for small separations. While this effect is localized at small separations in the correlation function, it can alter the power spectrum at small wavenumbers (large scales) and results in a modification of Poisson stochasticity (Mo & White 1996; Sheth & Lemson 1999; Smith, Scoccimarro & Sheth 2007; Baldauf et al. 2013) consistent with the sub-Poissonian noise measured in the clustering of simulated dark matter haloes (Casas-Miranda et al. 2002; Seljak, Hamaus & Desjacques 2009; Hamaus et al. 2010; Manera & Gaztañaga 2011). In addition, exclusion effects strongly suppress the non-physical k^0 tail of the one-halo term (Smith, Desjacques & Marian 2011).

Besides the exclusion effects, there are distinct, non-linear bias effects just outside the exclusion region which, due to their localization, also contribute to the power spectrum on large scales and for which the bias expansion converges very slowly. The exclusion region and the non-linear bias bump beyond are important for precision models of the halo–halo correlation function in the transition region between the one- and two-halo terms in the halo model. Thus, a better understanding of these regions will likely improve the modelling of the matter power spectrum or correlation function in this regime, which is very important for weak lensing or galaxy–galaxy lensing studies, since this signal is large and not yet dominated by the fully non-perturbative one-halo term.

Dark matter haloes are seeded by overdense regions in Lagrangian space (so called proto-haloes) that subsequently collapse to form the virialized late-time Eulerian haloes. Various assumptions can be made to describe the relation between the proto-haloes and the underlying

★ E-mail: codis@cita.utoronto.ca

Gaussian density field. Our perfect knowledge of the N-point statistics of the Gaussian field allows us to calculate all possible statistics of transformations of the Gaussian field. In this paper, we will consider the peak model (Bardeen et al. 1986; Regos & Szalay 1995), in which proto-haloes are associated with the maxima of the smoothed underlying field. To simplify the calculations and understanding, but without losing much of the phenomenology, we will consider volume exclusion effects associated with peaks in one spatial dimension, following Lumsden, Heavens & Peacock (1989) and Coles (1989). The 1D approach keeps the calculation simple, reducing the number of field variables to be considered at each point from 10 in 3D to 3 in 1D.

The paper is organized as follows. In Section 2, the general mathematical formalism that defines peak–peak correlations functions in dimension d, together with their numerical implementation are described. Section 3 presents the result on the small-scale exclusion zone of peaks obtained by numerical integration. The analytical large-scale bias expansion of the two-point correlation function of peaks is then discussed in Section 4. Section 5 incorporates the effect of the Zel'dovich displacement of the peaks and their velocity statistics. Finally, Section 6 wraps up.

2 FORMALISM AND NUMERICAL IMPLEMENTATION

The formalism of cosmological density peaks, which builds on the Kac–Rice formula Kac (1943) and Rice (1945) was laid down in Bardeen et al. (1986). Following Pogosyan et al. (2009), in d dimensions, for a given (overdensity) field ρ, we define the moments

$$\sigma_0{}^2 = \langle \rho^2 \rangle, \quad \sigma_1{}^2 = \langle (\nabla\rho)^2 \rangle, \quad \sigma_2{}^2 = \langle (\Delta\rho)^2 \rangle. \tag{1}$$

Combining these moments, we can build two characteristic lengths $R_0 = \sigma_0/\sigma_1$ and $R_\star = \sigma_1/\sigma_2$, as well as the spectral parameter

$$\gamma = \frac{\sigma_1{}^2}{\sigma_0\sigma_2}. \tag{2}$$

We choose to normalize the field and its derivatives to have unit variances:

$$x = \frac{1}{\sigma_0}\rho, \quad x_i = \frac{1}{\sigma_1}\nabla_i\rho, \quad x_{ij} = \frac{1}{\sigma_2}\nabla_i\nabla_j\rho. \tag{3}$$

In general, while $\mathcal{P}(\boldsymbol{X})$ designates the one-point probability density (PDF), $\mathcal{P}(\boldsymbol{X}, \boldsymbol{Y})$ will denote the joint PDF for the normalized field and its derivatives, $\boldsymbol{X} = \{x, x_{ij}, x_i\}$ and $\boldsymbol{Y} = \{y, y_{ij}, y_i\}$, at two prescribed comoving locations ($\boldsymbol{r}_x$ and $\boldsymbol{r}_y$ separated by a distance $r = |\boldsymbol{r}_x - \boldsymbol{r}_y|$). In the particular case of Gaussian initial conditions, this joint PDF is the multivariate normal

$$\mathcal{N}(\boldsymbol{X}, \boldsymbol{Y}) = \frac{\exp\left[-\frac{1}{2}\begin{pmatrix}\boldsymbol{X}\\ \boldsymbol{Y}\end{pmatrix}^{\mathrm{T}} \cdot \boldsymbol{C}^{-1} \cdot \begin{pmatrix}\boldsymbol{X}\\ \boldsymbol{Y}\end{pmatrix}\right]}{\det|\boldsymbol{C}|^{1/2}(2\pi)^{(d+1)(d+2)/2}}, \tag{4}$$

where $\boldsymbol{C}_0 \equiv \langle \boldsymbol{X}\cdot\boldsymbol{X}^{\mathrm{T}} \rangle$ and $\boldsymbol{C}_\gamma \equiv \langle \boldsymbol{X}\cdot\boldsymbol{Y}^{\mathrm{T}} \rangle$ are the diagonal and off-diagonal components of the covariance matrix

$$\boldsymbol{C} = \begin{pmatrix} \boldsymbol{C}_0 & \boldsymbol{C}_\gamma \\ \boldsymbol{C}_\gamma^{\mathrm{T}} & \boldsymbol{C}_0 \end{pmatrix}. \tag{5}$$

All these quantities depend on the separation vector $\boldsymbol{r}$ only because of homogeneity. Isotropy further implies that they depend on the modulus $r = |\boldsymbol{r}|$ solely. Equation (4) is sufficient to compute the expectation of any quantity involving the fields and its derivatives up to second order. In particular, the two-point correlation $\xi_{\mathrm{crit}}(r, \nu)$ of (signed) critical points at threshold ν separated by r is given by

$$1 + \xi_{\mathrm{crit}}(r, \nu) = \frac{\langle n_{\mathrm{crit}}(\boldsymbol{X}) n_{\mathrm{crit}}(\boldsymbol{Y}) \rangle}{\langle n_{\mathrm{crit}}(\boldsymbol{X}) \rangle^2}, \tag{6}$$

where the Klimontovich or 'localized' density for a signed critical point reads

$$n_{\mathrm{crit}}(\boldsymbol{X}) = \left(\frac{\sigma_2}{\sigma_1}\right)^d \det(x_{ij})\delta_{\mathrm{D}}(x_i)\delta_{\mathrm{D}}(x-\nu). \tag{7}$$

This density is formally zero unless the condition for a critical point is satisfied. The multiplicative factor of $(\sigma_1/\sigma_2)^d$, which has dimension of length^{-d}, ensures that the ensemble average

$$\langle n_{\mathrm{crit}}(\boldsymbol{X}) \rangle = \int \mathrm{d}\boldsymbol{X} \det(x_{ij})\delta_{\mathrm{D}}(x_i)\delta_{\mathrm{D}}(x-\nu)\mathcal{P}(\boldsymbol{X}) \equiv \bar{n}_{\mathrm{crit}}(\nu), \tag{8}$$

which appears in the denominator of equation (6), equals the average number density of critical points at threshold ν. The ensemble average

$$\langle n_{\mathrm{crit}}(\boldsymbol{X}) n_{\mathrm{crit}}(\boldsymbol{Y}) \rangle = \int \mathrm{d}\boldsymbol{X} \int \mathrm{d}\boldsymbol{Y}\, \mathcal{P}(\boldsymbol{X}, \boldsymbol{Y}) \det(x_{ij})\delta_{\mathrm{D}}(x_i)\delta_{\mathrm{D}}(x-\nu)\det(y_{ij})\delta_{\mathrm{D}}(y_i)\delta_{\mathrm{D}}(y-\nu), \tag{9}$$

is the cross-correlation. Since the integrand is simply a polynomial function of the variables, this integral can be fully carried out analytically. For peaks, an additional constraint on the sign of the second derivatives is required. As a consequence, the peak two-point correlation becomes

$$1 + \xi_{\mathrm{pk}}(r, \nu) = \frac{\langle n_{\mathrm{pk}}(\boldsymbol{X}) n_{\mathrm{pk}}(\boldsymbol{Y}) \rangle}{\langle n_{\mathrm{pk}}(\boldsymbol{X}) \rangle^2}. \tag{10}$$

where the localized peak number density $n_{\rm pk}(\boldsymbol{X})$,

$$n_{\rm pk}(\boldsymbol{X}) = \left(\frac{\sigma_2}{\sigma_1}\right)^d |\det(x_{ij})|\delta_{\rm D}(x_i)\Theta_{\rm H}(-\lambda_i)\delta_{\rm D}(x-\nu), \tag{11}$$

implements the peak condition. In odd dimensions (e.g $d = 1$), $|\det(x_{ij})| = -\det(x_{ij})$ because the determinant is negative at the peaks and it is understood that, for $d > 1$, $\delta_{\rm d}(x_i)$ stands for $\prod_{i\le d}\delta_{\rm D}(x_i)$, while $\Theta_{\rm H}(-y_{ii})$ means $\prod_{l\le d}\Theta_{\rm H}(-\lambda_l)$, with $\{\lambda_l\}_l$ being the eigenvalues of the Hessian. Because of these inequalities, the integral typically is not analytical anymore.

It has to be noted that contrary to peaks, the number density of signed critical points is not restricted to be positive. In particular, for Gaussian statistics, the number density of peaks and minima are related via $n_{\rm pk}(\nu) = n_{\rm min}(-\nu)$ so that $n_{\rm crit}(\nu)$ (which is nothing but the alternating sum of minima and peaks $n_{\rm min}(\nu) - n_{\rm pk}(\nu)$) is positive for $\nu < 0$ and negative for $\nu > 0$. In particular, $\xi_{\rm crit}$ is then expected to diverge for $\nu = 0$ and unlike peaks, it is not restricted to be above -1.

In d dimension, we define the conditional probability that x_{ij} and y_{ij} satisfy the PDF, subject to the condition that $x_i = y_i = 0$ and $x = y = \nu$ and resort to Monte Carlo methods in MATHEMATICA in order to evaluate numerically equation (10). Namely, we draw random numbers of dimension $d(d+1)$ from the conditional probability that x_{ij} and y_{ij} satisfy the PDF, subject to the condition that $x_i = 0$ and $x = y = \nu$ (using `RandomVariate`). For each draw $^{(k)}$, if $\lambda_l(x_{ij}^{(k)}) < 0$ and $\lambda_l(y_{ij}^{(k)}) < 0$ ($l \le d$), we keep the sample and evaluate $\det(x_{ij}^{(k)})\det(y_{ij}^{(k)})$ and otherwise we drop it; eventually,

$$\langle n_{\rm pk}(\boldsymbol{X}) n_{\rm pk}(\boldsymbol{Y})\rangle \approx \frac{1}{N}\sum_{k\in\mathcal{S}}\left[\det\left(x_{ij}^{(k)}\right)\det\left(y_{ij}^{(k)}\right)\right]\times\mathcal{P}(x=y=\nu, x_i=y_i=0), \tag{12}$$

where N is the total number of draws, and $\mathcal{S}$ is the subset of the indexes of draws satisfying the constraints on the eigenvalues. The same procedure can be applied to evaluate the denominator $\left\langle n_{\rm pk}(\boldsymbol{X})\right\rangle \equiv \bar{n}_{\rm pk}(\nu)$. Equation (10) then yields $\xi_{\rm pk}(r,\nu)$. This algorithm is embarrassingly parallel and can be easily generalized, for instance, to the computation of the correlation function $\xi_{\rm pk}(r, >\nu)$ of peaks above a given threshold in density and to arbitrary dimension d. In practice, it is fairly efficient as the draw is customized to the shape of the underlying Gaussian PDF. For $d = 1$ considered in this work, this brute force Monte Carlo method converges relatively quickly. Namely, we use one million draws for each evaluation of the correlation function in this work. This number is sufficient to reach percent precision accuracy. Obviously, if correlation function above a given threshold are considered, the required number of draws is larger and increases with the value of the threshold (as the event $x > \nu$ becomes rarer).

3 SMALL SCALES: PEAK–PEAK EXCLUSION

Here and henceforth, we will assume Gaussian initial conditions such that $\mathcal{P}(\boldsymbol{X},\boldsymbol{Y}) = \mathcal{N}(\boldsymbol{X},\boldsymbol{Y})$. In 1D, the block matrices that make up the covariance matrix are

$$\boldsymbol{C}_0 = \begin{pmatrix} 1 & 0 & -\gamma \\ 0 & 1 & 0 \\ -\gamma & 0 & 1 \end{pmatrix}, \quad \boldsymbol{C}_\gamma = \begin{pmatrix} \gamma_{00} & \gamma_{01} & \gamma_{02} \\ \gamma_{01} & \gamma_{11} & \gamma_{12} \\ \gamma_{02} & \gamma_{12} & \gamma_{22} \end{pmatrix}, \tag{13}$$

where the γ_{ij}s represent the correlations between the field and its derivatives at two points separated by a comoving distance r, e.g. $\gamma_{22} = \langle x_{11}y_{11}\rangle$. These γ_{ij}s are not independent. The following relations are established via integrations by part: $\gamma_{10} = -\gamma_{01}$, $\gamma_{21} = -\gamma_{12}$, $\gamma_{20} = -\gamma\gamma_{11}$. The $\gamma_{ij}(r)$ are known function of r given by the moments of the two fields and their derivatives:

$$\gamma_{ij}(r) = \frac{1}{\sigma_i\sigma_j}\int {\rm d}k\, \exp(\imath kr)(\imath k)^i(-\imath k)^j P_{\rm s}(k) \quad i \le j, \tag{14}$$

with $P_{\rm s}(k)$ the power spectrum of δ smoothed with a filter function (assumed Gaussian throughout this work). On expanding $\gamma_{ij}(r)$ at small separations $r \ll R$ and substituting the spectral moments

$$\sigma_l^2 = \frac{1}{\pi}\int_0^\infty {\rm d}k\, k^{2l} P_{\rm s}(k), \tag{15}$$

it follows that

$$\gamma_{ij}(r) = \frac{(-1)^{l-i}}{\sigma_i\sigma_j}\sum_{k=0}^{\infty}\frac{(-1)^k}{(2k)}\left(\frac{r}{R}\right)^{2k}!\sigma_{l+k}^2 \qquad (i+j=2l), \tag{16}$$

$$\gamma_{ij}(r) = \frac{(-1)^{1+l-i}}{\sigma_i\sigma_j}\sum_{k=0}^{\infty}\frac{(-1)^k}{(2k+1)!}\left(\frac{r}{R}\right)^{2k+1}\sigma_{l+k+1}^2 \quad (i+j=2l+1), \tag{17}$$

where $\tilde{r} = r/R$ is the separation in units of the smoothing length R. The determinant of the covariance matrix $\boldsymbol{C}$ is given at leading order in the separation r by $(r/R)^{18} \times g(\{\sigma_i\}_{0\ge i\ge 5})$ where $g = \left(\sigma_2^6 - \left(2\sigma_1^2\sigma_3^2 + \sigma_0^2\sigma_4^2\right)\sigma_2^2 + \sigma_0^2\sigma_3^4 + \sigma_1^4\sigma_4^2\right)\times \left(\sigma_3^6 - \left(2\sigma_2^2\sigma_4^2 + \sigma_1^2\sigma_5^2\right)\sigma_3^2 + \sigma_1^2\sigma_4^4 + \sigma_2^4\sigma_5^2\right)/74\,649\,600\sigma_0^4\sigma_1^4\sigma_2^4$ does not depend on the separation. Indeed, three eigenvalues of $\boldsymbol{C}$ are

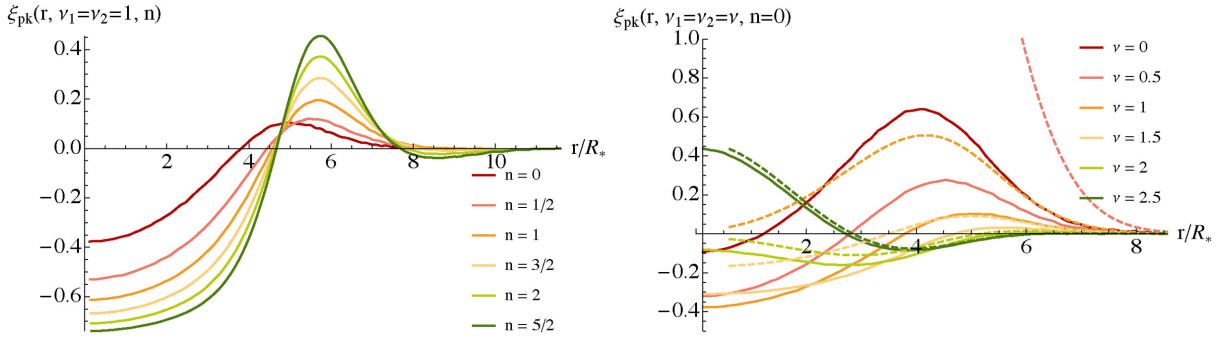

Figure 1. Left-hand panel: 1D correlation function of peaks of height $\nu = 1$ as a function of $r/R_\star$ for different spectral index n evaluated by Monte Carlo realizations of the peak constraint. Right-hand panel: same as left-hand panel, but the spectral index is held fixed at $n = 0$ while the peak height ν is varied between 0 and 2.5 as labelled. The dashed lines indicate the analytical 1D signed critical point correlation function. For $\nu > 2$, both the peak and signed critical points correlations are in very good agreement. Note that, for $\nu = 0$, the signed critical point correlation functions diverges (because the alternating sum of $\nu = 0$ critical points goes to zero) and is thus not shown on this plot.

singular, respectively scaling like r^{10}, r^6 and r^2 and corresponding to the eigendirections given by $(x - y)$, $(x_1 - y_1)$ and $(x_{11} - y_{11})$. This singularity proportional to r^{-18} is the reason why the limit $r \to 0$ is difficult to handle numerically. Analytically, this means that a series expansion to 18th order is needed for all terms. Note that Lumsden et al. (1989) only expand the covariance matrix to second order. Truncating the expansion at this order, we find that the determinant scales as r^{10} and the 11th element of the inverse as $\boldsymbol{C}_{11}^{-1} \propto r^{-4}$. Their expansion was thus not sufficient to account for the cancellations between terms at small separations.[1]

3.1 Correlation of 1D peaks of same height

We evaluate the two-point correlation function of $d = 1$ peaks upon applying the Monte Carlo method described above to equation (10). Results for a power-law power spectrum $P_s(k) = Ak^n$ are shown in the left-hand panel of Fig. 1 as a function of the spectral index n for a fixed peak height $\nu = 1$. The exclusion zone shrinks to smaller separations and becomes more pronounced as n is increased because the addition of small-scale power tends to sharpen the profile around local density maxima. In the right-hand panel of Fig. 1, we display $\xi_{pk}(r, \nu)$ as a function of peak height for a white noise power spectrum $n = 0$. For comparison, the dashed curves represent the two-point correlation of 1D signed critical points, which is obtained upon integrating equation (6) over the six field variables. Unsurprisingly, $\xi_{crit}(r, \nu)$ matches $\xi_{pk}(r, \nu)$ almost perfectly for prominent peaks ($\nu \gtrsim 2$) since, in this regime, a critical point is nearly always a local maximum.

Interestingly, the two-point correlation $\xi_{crit}(r, \nu)$ is fully analytical regardless of the underlying density power spectrum. For the sake of readability however, we will not display its full expression here. Nevertheless, we can take advantage of this analytic result, together with the fact that $\xi_{pk}(r, \nu)$ agrees very well with its genus-like counterpart $\xi_{crit}(r, \nu)$ at high threshold, to get insights into the short distance behaviour of the peak correlation function. The low-r limit of the two-point correlation function of signed critical points separated by r is given by

$$1 + \xi_{crit}(r, \nu) = \frac{e^{\frac{(2\gamma^2-1)\nu^2}{2(\gamma^2-1)}} \left(\gamma_\#^2 \left(\gamma^2\gamma_\star^4 \left(\gamma^2 + \nu^2 - 1\right) - 2\gamma^2\gamma_\star^2 \left(\gamma^2 + \nu^2 - 1\right) + \gamma^2 \left(\nu^2 + 1\right) - 1\right) + \left(\gamma^2 - 1\right)^2\right)}{12\gamma^3 \left(1 - \gamma^2\right)^{5/2} \nu^2 \gamma_\#^2 \sqrt{1 - \gamma_\star^2}\gamma_\star^3} + \mathcal{O}(r/R), \tag{18}$$

where we define the following extra shape parameters $\gamma_\star = \sigma_2^2/\sigma_1/\sigma_3$ and $\gamma_\# = \sigma_3^2/\sigma_2/\sigma_4$.

For a power-law power spectrum $P_s(k) = Ak^n$, with spectral index $n > -1$, and a density field filtered with a Gaussian kernel of radius R, the $\gamma_{ij}(r)$ are given by

$$\gamma_{00}(r) = {}_1F_1\left(\frac{n+1}{2}; \frac{1}{2}; -\frac{r^2}{4R^2}\right),$$

$$\gamma_{11}(r) = {}_1F_1\left(\frac{n+3}{2}; \frac{1}{2}; -\frac{r^2}{4R^2}\right),$$

$$\gamma_{22}(r) = {}_1F_1\left(\frac{n+5}{2}; \frac{1}{2}; -\frac{r^2}{4R^2}\right), \tag{19}$$

and $\gamma_{02}(r) = -\gamma\gamma_{11}(r)$. Here, ${}_1F_1$ is the Kummer confluent hypergeometric function and

$$\sigma_l^2 \propto R^{-1-n-2l}\, \Gamma\left(\frac{1}{2} + \frac{n}{2} + l\right). \tag{20}$$

[1] Note that this difficulty arises only in the low-r behaviour and therefore does not affect the full computations done in that paper.

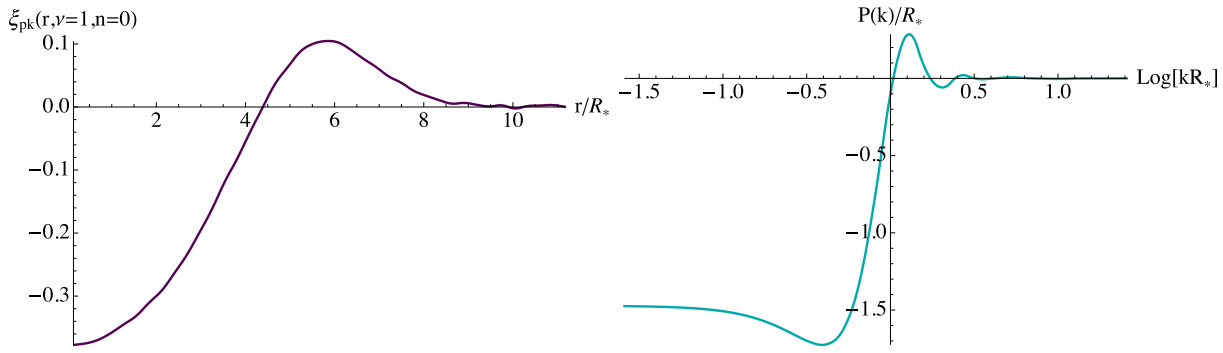

Figure 2. Left-hand panel: Monte Carlo estimation of the two-point correlation function of 1D peaks $\xi_{\rm pk}(r,\,\nu)$. The results is shown as a function of $r/R_\star$ assuming $n=0$ and a threshold $\nu=1$. Right-hand panel: corresponding power spectrum $P_{\rm pk}(k,\,\nu)$. The exclusion zone seen at short distance in the left-hand panel makes the 1D peak power spectrum sub-Poissonian at small wavenumber (large separation).

Therefore, the shape parameters are $\gamma=(1+n)/(3+n)$, $\gamma_\star=(3+n)/(5+n)$ and $\gamma_\#=(5+n)/(7+n)$, and the determinant of $\boldsymbol{C}$ thus scales like $\gamma^2(2-\gamma^2)(1-\gamma^2)^{-3}(r/R)^{18}/18\,662\,400$, as advertised at the beginning of this section. Note that, in this work, all the figures display the separation in units of $\tilde{r}=r/R_\star$ instead of the smoothing length R as $R_\star$ represents the typical distance between extrema (Bardeen et al. 1986) and is therefore more meaningful. In the case where $n=0$, the low-r behaviour of the two-point correlation function of signed critical points can be written as follows

$$1+\xi_{\rm crit}(\tilde{r},\,\nu,\,n=0)=\frac{e^{\frac{\nu^2}{4}}\left(3\nu^2+8\right)}{8\sqrt{3}\nu^2}+\frac{e^{\frac{\nu^2}{4}}\left(128-15\nu^4\right)\tilde{r}^2}{1920\sqrt{3}\nu^2}+\frac{e^{\frac{\nu^2}{4}}\left(15\nu^4-64\right)\tilde{r}^4}{184\,320\sqrt{3}}+\mathcal{O}\left(\tilde{r}^5\right)\,, \tag{21}$$

which makes clear that $\xi_{\rm crit}$ diverges for $\nu=0$. The dependence of the low-r expansion with the spectral index n for peaks of height $\nu=1$ reads

$$1+\xi_{\rm crit}(\tilde{r},\,\nu=1,\,n)=\frac{e^{\frac{1}{4}-\frac{n}{4}}(n+3)\left(n^2+4n+11\right)}{24(n+1)\sqrt{n^2+4n+3}}+\frac{e^{\frac{1}{4}-\frac{n}{4}}(n+3)\left(-25n^4+40n^3+410n^2+1464n+1695\right)\tilde{r}^2}{86\,400(n+1)\sqrt{n^2+4n+3}}+\mathcal{O}\left(\tilde{r}^3\right), \tag{22}$$

which shows that the exclusion zone is more pronounced for high values of the spectral index. The same trend was also seen for peaks in the left-hand panel of Fig. 1. As shown in Baldauf et al. (2013), the small-scale peak repulsion in the configuration space correlation function can have a significant impact on the power spectrum at small wavenumbers. To emphasize this point, Fig. 2 displays, in the left-hand panel, the 1D peak correlation function as a function of $\tilde{r}=r/R_\star$ assuming $n=0$ and a threshold $\nu=1$ and, in the right-hand panel, the corresponding power spectrum obtained by a simple Fourier transform of the real space Monte Carlo result

$$P_{\rm pk}(k)=2\int_0^\infty {\rm d}r\,\xi_{\rm pk}(r)\cos(kr)\,. \tag{23}$$

In this particular case, the power spectrum is approximately white for all wavenumbers $k\lesssim 1/R_\star$, with $P_{\rm pk}(k\lesssim R_\star,\,\nu=1)\approx -1.5R_\star$.

3.2 How strong is the small-scale exclusion?

So far, we have assumed that the peaks under consideration have exactly the same height. This is clearly a very special case, since a realistic sample of haloes is likely to be made up by a range of masses or smoothing scales and thus of different peak heights ν. As we have seen in Fig. 1, the exclusion region is often reduced to an anti-correlation, in the sense that $1+\xi_{\rm pk}(r,\,\nu)$ does not reach zero at the origin. In order to ascertain whether this is a robust feature, we have also computed the correlation function of 1D peaks and critical points with different heights $\nu_1=\nu-\Delta\nu/2$ and $\nu_2=\nu+\Delta\nu/2$, where $\Delta\nu>0$ is the height difference. For the critical points, we have at small separations

$$1+\xi_{\rm crit}\left(\tilde{r},\,\nu-\frac{\Delta\nu}{2},\,\nu+\frac{\Delta\nu}{2},\,n=0\right)=\sqrt{3}\left[\frac{\alpha_8(\nu,\,\Delta\nu)\Delta\nu^2}{\tilde{r}^8\left(\Delta\nu^2-4\nu^2\right)}+\frac{\alpha_6(\nu,\,\Delta\nu)\Delta\nu^2}{\tilde{r}^6\left(\Delta\nu^2-4\nu^2\right)}+\frac{\alpha_4(\nu,\,\Delta\nu)\Delta\nu^2}{\tilde{r}^4\left(\Delta\nu^2-4\nu^2\right)}+\frac{\alpha_2(\nu,\,\Delta\nu)\Delta\nu^2}{5\tilde{r}^2\left(\Delta\nu^2-4\nu^2\right)}\right.$$
$$\left.+\frac{\alpha_0(\nu,\,\Delta\nu)}{\left(\Delta\nu^2-4\nu^2\right)}\right]\exp\left[\frac{\nu^2}{4}+\frac{7\Delta\nu^2}{80}-\frac{9\Delta\nu^2}{5\tilde{r}^2}+\frac{27\Delta\nu^2}{\tilde{r}^4}-\frac{324\Delta\nu^2}{\tilde{r}^6}\right]+\mathcal{O}(\tilde{r}), \tag{24}$$

where the functions $\alpha_{2n}(\nu,\,\Delta\nu)$ for n between 0 and 4 are given in Appendix A and

$$\alpha_0(\nu,\,\Delta\nu=0)=\left(\frac{1}{8}+\frac{1}{3\nu^2}\right). \tag{25}$$

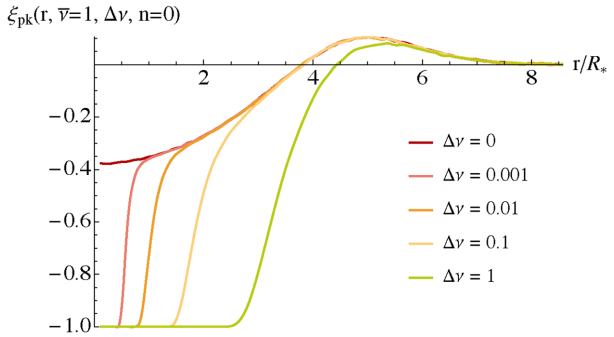

Figure 3. The two-point correlation function of 1D peaks with height $\nu_1 = 1 - \Delta\nu/2$ and $\nu_2 = 1 + \Delta\nu/2$ is shown as a function of the height difference $\Delta\nu$ as labelled in the figure. A fixed value of $\bar{\nu} \equiv (\nu_1 + \nu_2)/2 = 1$ was assumed. All the correlation functions were estimated using the Monte Carlo method described in Section 2.

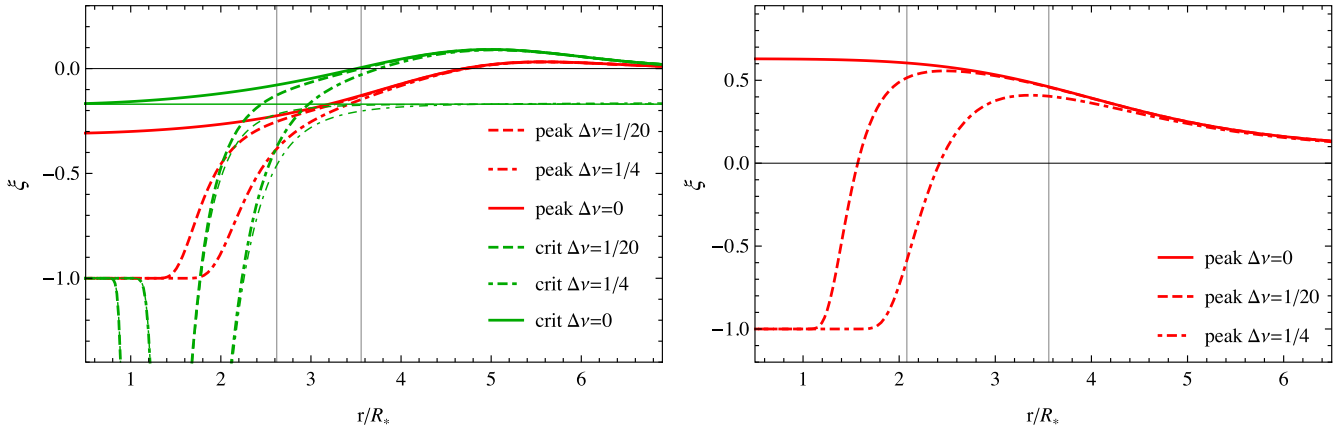

Figure 4. Left-hand panel: correlation function of peaks (red) and critical points (green) for $\bar{\nu} = 3/2$ and for $\Delta\nu = 0$ (solid), $\Delta\nu = 1/10$ (dashed) and $\Delta\nu = 1/4$ (dot–dashed). The scales, where the $\Delta\nu = 0$ and $\Delta\nu \neq 0$ cases deviate are similar for peaks and critical points. For the critical points, we overplot the low-r expansion equation (24). This expansion provides a good description of the low-r behaviour up to 2–3 $R_\star$. The vertical lines indicate the respective $r_{1\,\mathrm{per\,cent}}$ scales, and provide a useful estimate of the scale where the $\Delta\nu = 0$ and $\Delta\nu \neq 0$ cases start to deviate in the full calculation. Right-hand panel: same as left-hand panel for a projected ΛCDM power spectrum with $R = 2\,h^{-1}$ Mpc.

Comparing this expression to equation (21) above, we see that for unequal heights, inverse powers of the separation arise. The r^{-6} term in the exponential drives the correlation function to -1 on very small scales. We can estimate where the leading inverse power in the exponent causes a one percent correction to $1 + \xi$

$$r_{1\,\mathrm{per\,cent}} \approx (180\Delta\nu)^{1/3}\, R_\star. \tag{26}$$

Numerical results for peaks are shown in Fig. 3 for different choices of $\Delta\nu$. While the correlation $1 + \xi_{pk}(r, \nu_1, \nu_2)$ of peaks of different heights tends towards zero at small separation, it converges towards a finite non-zero value when the peaks have exactly the same height. In Fig. 4, we compare the exclusion of peaks and critical points to the approximation of equation (24). The scales where the finite separation results deviate from the equal height case are approximately the same for peaks and critical points and $r_{1\,\mathrm{per\,cent}}$ is a good indicator of this scale. We also compare the size of the exclusion region for peaks in a projected cold dark matter (ΛCDM) density field with the corresponding $r_{1\,\mathrm{per\,cent}}$ and find equally good agreement.[2] Therefore, the behaviour of ξ_{pk} in the limit $r \to 0$ strongly depends on the peak height difference. This can be easily understood as follows: consider two peaks infinitesimally close to each other. Very stringent constraints on the first and second derivatives of the density field are thus required to bridge them. Clearly, the constraints will be more draconian the larger the height difference. Therefore, this configuration becomes increasingly unlikely with increasing $\Delta\nu > 0$, and thus $1 + \xi_{pk}(r, \nu_1, \nu_2)$ rapidly drops to zero as the separation decreases. The same behaviour is, of course, expected to hold for peaks with different smoothing scales and for integrals

[2] For the peaks in a projected ΛCDM power spectrum, we smooth the underlying 3D power spectrum with a Gaussian filter and then consider the peaks along one of the coordinate axis (taken to be the z-axis without loss of generality). The effective 1D input power spectrum entering equation (14) is then

$$P_{s,1D}(k_z) = \int \frac{\mathrm{d}k_x \mathrm{d}k_y}{(2\pi)^2} P_{3D}\left(\sqrt{k_x^2 + k_y^2 + k_z^2}\right) W^2\left(\sqrt{k_x^2 + k_y^2 + k_z^2}R\right)\,, \tag{27}$$

where $W(kR) = e^{-k^2R^2/2}$ is the Gaussian window.

over bins in peak height. Note that the short distance behaviour of the peak correlation with fixed height does not follow the exponential suppression $\exp(-R_\star^2/r^2)$ found by Lumsden et al. (1989) for peaks above a threshold.[3]

4 LARGE SCALES: PERTURBATIVE BIAS EXPANSION

Perturbative bias expansions have been widely used to predict clustering statistics of dark matter haloes and galaxies. However, no study so far has explored the convergence properties of these series because of the highly non-linear (non-perturbative) effects induced by small-scale exclusion. In this section, we wish to address this issue using the clustering of 1D peaks as a proxy for the two-halo term.

4.1 Methodology

As discussed in Desjacques (2013), the two-point correlation function of 3D peaks can be computed from a perturbative, local (peak) bias expansion in which the coefficients (bias parameters) are computed from a generalized peak-background split ansatz. This procedure is fairly general and it applies to any 'point' process of a Gaussian (and possibly non-Gaussian) random field. Therefore, it should certainly describe the two-point function of our 1D peak. In 1D, the perturbative bias expansion is constructed from three rotationally invariant quantities, i.e. the rescaled field x, x_1^2 and x_{11} [in the notation of Bardeen et al. (1986), $x=\nu$, $x_1=\eta/\sigma_1$ and $x_{11}=-x$]. Following equation (11), the 'localized' number density of peaks of height ν then is

$$n_{\rm pk}(\boldsymbol{X}) = \frac{\sigma_2}{\sigma_1}|x_{11}|\delta_{\rm D}(x_1)\delta_{\rm D}(x-\nu)\Theta_{\rm H}(-x_{11}). \tag{28}$$

The knowledge of $n_{\rm pk}(\nu)$ suffices to derive the bias parameters associated with this point process at all orders. Namely, the probability density for the variables $\boldsymbol{X}=(x,x_{11},x_1)$ is the product of a bivariate normal $\mathcal{N}(x,x_{11})$ with a chi-square distribution $\chi_1^2(x_1^2)$ with one degree of freedom. To construct the perturbative bias expansion, we proceed as in Desjacques (2013) and perturb the localized peak number density (the peak-background split). This perturbation can be represented as a series in the appropriate orthogonal polynomials, i.e. Hermite polynomials for $\mathcal{N}(x,x_{11})$ and generalized Laguerre polynomials for $\chi_1^2(x_1^2)$. The perturbative bias expansion describing 1D peaks thus is

$$\begin{aligned}\delta_{\rm pk}(r) &= \sum_{i,j,k}\frac{\sigma_0^i\sigma_2^j\sigma_1^{2k}}{i!j!}\frac{\Gamma(1/2)}{\Gamma(k+1/2)}b_{ij}\chi_k H_{ij}(x(r),-x_{11}(r))L_k^{(-1/2)}(x_1(r))\\ &= \sigma_0 b_{10}x(r)-\sigma_2 b_{01}x_{11}(r)+\frac{1}{2}\sigma_0^2 b_{20}\left[x^2(r)-1\right]-\sigma_0\sigma_2 b_{11}x(r)x_{11}(r)+\frac{1}{2}\sigma_2^2 b_{02}\left[x_{11}^2(r)-1\right]+\sigma_1^2\chi_1\left[x_1^2(r)-1\right]+\ldots,\end{aligned} \tag{29}$$

where $\delta_{\rm pk}$ is the mean field peak overabundance, and r is the 1D comoving coordinate. The factor of unity in the quadratic terms removes the zero-lag contributions. The bias parameters are the ensemble averages

$$\sigma_0^i\sigma_2^j b_{ij} = \frac{1}{\bar{n}_{\rm pk}(\nu)}\int {\rm d}\boldsymbol{X}\, n_{\rm pk}(\boldsymbol{X})\mathcal{N}(\boldsymbol{X})\, H_{ij}(x,-x_{11}), \tag{30}$$

$$\sigma_1^{2k}\chi_k = \frac{(-1)^k}{\bar{n}_{\rm pk}(\nu)}\int {\rm d}\boldsymbol{X}\, n_{\rm pk}(\boldsymbol{X})\mathcal{N}(\boldsymbol{X})\, L_k^{(-1/2)}(x_1^2/2). \tag{31}$$

Here, H_{ij} and $L_k^{(-1/2)}$ are bivariate Hermite and Laguerre polynomials, respectively so that χ_k is simply $\chi_k=(-1/2)^k(2k-1)!!/(k!\sigma_1^{2k})$ and $H_{ij}(x,-x_{11})=\mathcal{N}^{-1}(x,x_{11})(-\partial_x)^i\left(\partial_{x_{11}}\right)^j\mathcal{N}(x,x_{11})$ has been commonly defined for the peak curvature $-x_{11}$. For instance,

$$H_{10}(x,-x_{11}) = \frac{x+\gamma x_{11}}{1-\gamma^2} \tag{32}$$

$$H_{01}(x,-x_{11}) = -\frac{\gamma x+x_{11}}{1-\gamma^2}. \tag{33}$$

The average peak number density entering equations (30 and 31) is given by

$$\begin{aligned}\bar{n}_{\rm pk}(\nu) &= \frac{\sigma_2}{\sigma_1}\int {\rm d}\boldsymbol{X}\,\mathcal{N}(\boldsymbol{X})\,|x_{11}|\delta_{\rm D}(x_1)\delta_{\rm D}(x-\nu)\Theta_{\rm H}(-x_{11}),\\ &= \frac{\sigma_2}{\sigma_1}\frac{1}{\sqrt{2\pi}}\int {\rm d}x_{11}\,|x_{11}|\mathcal{N}(\nu,x_{11})\Theta_{\rm H}(-x_{11}),\\ &= \frac{\sigma_2}{\sigma_1}\left\{\frac{1}{2}\gamma\nu\left[1+{\rm Erf}\left(\frac{\gamma\nu}{\sqrt{2-2\gamma^2}}\right)\right]+\sqrt{\frac{1-\gamma^2}{2\pi}}e^{-\frac{\gamma^2\nu^2}{2(1-\gamma^2)}}\right\}\frac{e^{-\nu^2/2}}{2\pi},\\ &\equiv \frac{1}{2\pi R_\star}G(\gamma,\gamma\nu)e^{-\nu^2/2},\end{aligned} \tag{34}$$

where, again, $R_\star=\sigma_1/\sigma_2$. The peak bias expansion given by equation (29) is to be compared with the standard linear bias approach which

[3] As we have noted before, Lumsden et al. (1989) did not go to sufficiently high orders in small-scale separation to account for the cancellations of the elements of the covariance matrix leading to the correct low-r behaviour of the inverse covariance and determinant. This likely also invalidates their conclusions on the leading behaviour of the peak correlation function above threshold.

relates linearly the density of dark matter haloes to the dark matter density field

$$\delta_h(r) = \sigma_0 b\, x(r)\,, \tag{35}$$

where $b \equiv b_{10}$ is the usual linear bias parameter.

In 1D, we could also use x_1 rather than x_1^2 as independent variable. x_1 is normally distributed, so that the joint probability distribution reads $P_1(x, x_1, x_{11}) = \mathcal{N}(x, x_{11})\mathcal{N}(x_1)$, and the bias parameters χ_k, now associated with x_1, are

$$\begin{aligned}\sigma_1^k \chi_k &= \frac{1}{\bar{n}_{\rm pk}} \int {\rm d}\boldsymbol{X}\, \mathcal{N}(\boldsymbol{X})\, H_k(x_1) \\ &= (-1)^{k/2}\,(k-1)!! \qquad \text{if } k \text{ is even}\,.\end{aligned} \tag{36}$$

In both cases, we recover the same series expansion. Namely, on perturbing either $\mathcal{N}(x_1)$ or $\chi_1^2(x_1^2)$ with a long-wavelength perturbation x_{1l}, such that $x_1 \to x_1 + x_{1l}$ and $x_1^2 \to x_1^2 + x_{1l}^2$, we find (Desjacques 2013)

$$\text{(i)} \qquad \sum_{n=0}^{\infty} \frac{1}{n!}(\sigma_1^n \chi_n) x_{1l}^n = \sum_{k=0}^{\infty} \frac{1}{(2k)!}(-1)^k (2k-1)!!\, x_{1l}^{2k} = \sum_{k=0}^{\infty} \frac{(-1)^k}{2^k k!} x_{1l}^{2k}, \quad \text{(Hermite)}$$

$$\text{(ii)} \qquad \sum_{k=0}^{\infty} \frac{\Gamma(\alpha+1)}{\Gamma(\alpha+k+1)}(\sigma_1^{2k}\chi_k)\left(\frac{x_{1l}^2}{2}\right)^k = \sum_{k=0}^{\infty} \frac{2^k}{(2k-1)!!}(-1/2)^k \frac{(2k-1)!!}{k!}\left(\frac{x_{1l}^2}{2}\right)^k = \sum_{k=0}^{\infty} \frac{(-1)^k}{2^k k!} x_{1l}^{2k} \quad \text{(Laguerre)}.$$

In other words, we could equally work with the bias factors χ_k expressed either as Hermite or Laguerre. We could also have followed Gay, Pichon & Pogosyan (2012) and works with the variables $(z = (x + \gamma x_{11})/\sqrt{1-\gamma^2}, x_{11})$ which have the advantage of being statistically independent. In what follows, we will stick to the variable x_1^2.

The 1D peak two-point correlation $\xi_{\rm pk}(r)$ can be perturbatively computed from equation (29). In practice, one evaluates the ensemble average $\langle n_{\rm pk}(\boldsymbol{r}_x) n_{\rm pk}(\boldsymbol{r}_y)\rangle$, ensuring to discard all the terms involving zero-lag moments. At first order, this is

$$\xi_{\rm pk}(r) = b_{10}^2 \xi_0(r) + 2 b_{10} b_{01} \xi_1(r) + b_{01}^2 \xi_2(r)\,, \tag{37}$$

where

$$\xi_l(r) = \frac{1}{\pi}\int_0^{\infty} {\rm d}k\, k^{2l} P_{\rm s}(k) \times \begin{cases} \cos(kr) & l \text{integer} \\ \sin(kr) & l \text{half integer} \end{cases}. \tag{38}$$

Note that $\xi_i(r) = \sigma_i^2 \gamma_{ii}(r)$, where $\gamma_{ij}(r)$ is defined in equation (14). For Gaussian initial conditions (which we assume throughout this paper), the Nth-order contribution to $\xi_{\rm pk}(r)$ involves $N(N+1)/2$ distinct combinations of x and x_{11} correlators together with N^2 terms involving correlators of x_1^2. Therefore, the number of terms scales like N^2. Consequently, the 1D peak correlation up to Nth order involves $\mathcal{O}(N^3)$. All these contributions can be expressed as a product of the six possible connected two-point correlators $\langle x(\boldsymbol{r}_x) x(\boldsymbol{r}_y)\rangle$, $\langle x(\boldsymbol{r}_x) x_1(\boldsymbol{r}_y)\rangle$ etc. However, the coefficients are product of Nth-order bias parameters and change from term to term. Therefore, the bias perturbative expansion will be of limited use unless the bias coefficients can be computed quickly. In practice, exploiting the recurrence among the orthogonal polynomials can help reducing the computational cost.

4.2 Convergence in real and Fourier space

Armed with these results, we can assess the convergence properties of the 1D peak perturbative bias expansion. For illustrative purposes, we will consider a power-law power spectrum $P_{\rm s}(k) \propto k^n$ with $n = 0$ and a peak height $\nu = 1$. In the left-hand panel of Fig. 5, we compare the exact result (solid green curve) with the $N = 1$, 2, 5 and 10th order perturbative approximations (in colour). While the latter captures the excess correlation at a few $R_\star$ relatively well, the convergence to the exact result is fairly slow at shorter separations where exclusion effects become important. In any case, the peak bias expansion equation (29) performs significantly better than a 'local bias' approximation, in which only the dependence on $x(r)$ is retained in the perturbative series equation (29). The first and second-order 'local bias' approximations are shown as the black curves, and clearly furnish a poor fit to the exact result for $r/R_\star \lesssim$ a few.

The upper right-hand panel of Fig. 5 displays the resulting power spectra obtained by taking the Fourier transform of $\xi_{\rm pk}(r)$ and its various perturbative approximations. For the sake of comparison, the dotted black curve represents the first-order local bias approximation. Small-scale exclusion translates into a white-noise contribution in the limit $k \to 0$ which makes the shot-noise non-Poissonian, in agreement with the findings of Smith et al. (2007) and Baldauf et al. (2013). Note that such a k^0 tail also arises in the clustering of thresholded regions (Beltrán Jiménez & Durrer 2011). The magnitude of the white-noise correction changes with the order N of the approximation because it receives contributions from all orders. As shown in the previous section, deriving an analytic expression valid throughout the exclusion zone is practically impossible and, therefore, there is no hope to obtain exact expressions for these deviations from Poisson noise. The bottom right-hand panel of Fig. 5 displays the power spectra once the white noise correction $P_{\rm pk}(k=0)$ (which generally depends on the order N of the approximation) has been subtracted. The relatively slow convergence of the perturbative approximations to the 1D peak power spectrum towards the exact result reflects the behaviour seen in configuration space. We expect that these considerations also hold for the convergence

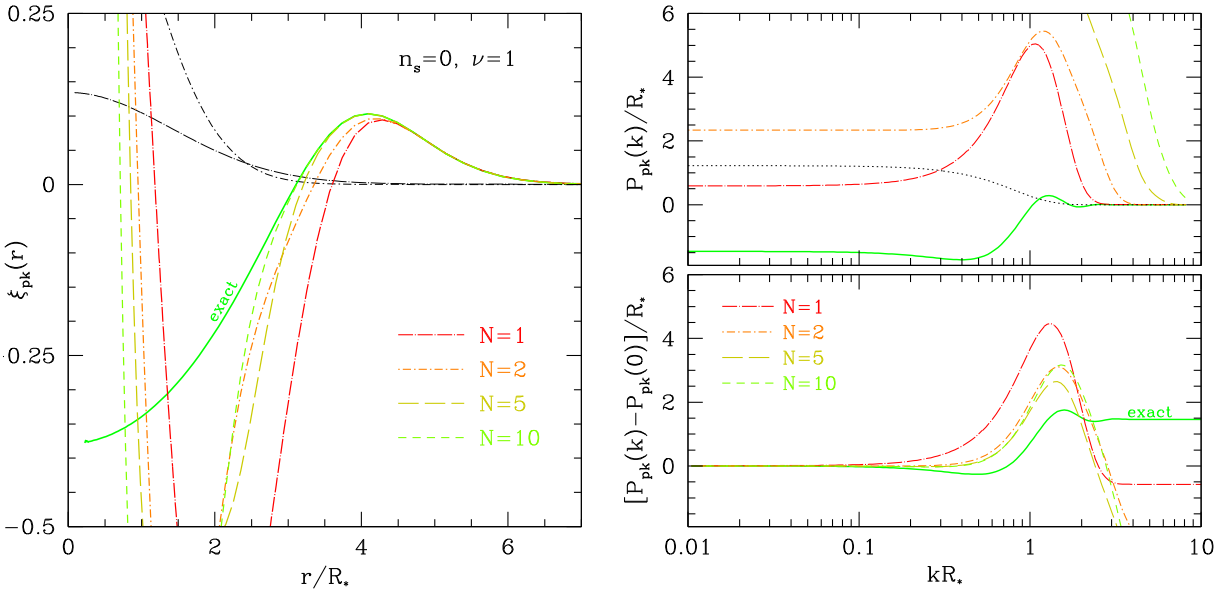

Figure 5. Left-hand panel: comparison between the exact correlation function of 1D peaks and perturbative series obtained upon truncating the peak bias expansion equation (29) at order of $N = 1$, 2, 5 and 10. For illustration, the black curves show linear and quadratic local bias approximations and perform significantly worse than the peak bias expansion. A white noise power spectrum with Gaussian filtering and a peak height $\nu = 1$ were assumed. Top right: exact peak power spectrum (solid) compared to various approximations obtained upon truncating the bias expansion at order of $N = 1$, 2, 5 and 10. For comparison, the dotted line represents the linear bias approximation. Bottom right: same as top panel but the zero-lag value $P_{\rm pk}(0)$ has been subtracted off from the power spectra. In all cases, a white noise power spectrum with Gaussian smoothing and a peak height of unity were assumed.

of perturbative bias expansions of actual dark matter haloes, even though the convergence rate may depend on the dimensionality and the shape of the density power spectrum.

5 DYNAMICS OF THE PEAKS

So far we have been concerned with peaks in Lagrangian space, but haloes are observed in Eulerian space, i.e. after gravitational evolution. In this section, we will identify peaks in Lagrangian space and move them according to their Zel'dovich displacement. The discrete tracer set generated in this way should be in close correspondence with the peaks identified in the evolved non-Gaussian field, or haloes in a more realistic setting. This is the approximation that was made in the 3D calculation of Desjacques et al. (2010). For that purpose, let us use the Lagrangian displacement Ψ to relate the Lagrangian peak position q to its final Eulerian position r

$$r_{\rm pk} = q_{\rm pk} + D_+ \Psi_{\rm pk}(q_{\rm pk}) \,, \tag{39}$$

where D_+ is the linear growth factor and the displacement satisfies the equation of motion

$$\Psi'' + \mathcal{H}\Psi' = -\nabla_r \phi \,, \tag{40}$$

where ϕ is the gravitational potential. The linear solution to this equation in three dimensions is known as the Zel'dovich approximation and describes ballistic evolution according to the initial velocity. We will assume that the peak displacement is related to the mean displacement of the peak patch, i.e. by $\Psi(k) = -\imath k/k^2 \delta(k) W_R(k)$, where $W_R(k)$ is the smoothing window. Due to the presence of the smoothing scale, we expect the Zel'dovich approximation to work better for the finite size peaks than for the matter field itself, which undergoes shell crossing. Conveniently, in one dimension, the Zel'dovich solution is the exact solution (Buchert 1989; Yoshisato, Matsubara & Morikawa 1998; McQuinn & White 2015).[4]

[4] From $[1 + \delta(r)]{\rm d}r = {\rm d}q$, we have $\delta(r) = 1/J - 1$ with $J = |1 + \nabla_q \Psi|$. Then, we can take the Eulerian divergence of the equation of motion

$$\nabla_r \left[\Psi'' + \mathcal{H}\Psi'\right] = \frac{3}{2}\mathcal{H}^2 \delta. \tag{41}$$

Rewriting the Eulerian as a Lagrangian derivative $\nabla_r = (1 + \nabla_q \Psi)^{-1} \nabla_q$ we finally have

$$\nabla_q \left[\Psi'' + \mathcal{H}\Psi'\right] = \frac{3}{2}\mathcal{H}^2 \nabla_q \Psi, \tag{42}$$

which is a linear equation for Ψ that can be solved exactly by $\Psi = D_+ \Psi_0$ before shell crossing, where D_+ is the linear growth.

5.1 Zel'dovich displacement of peaks

We can now write the Eulerian halo/peak overdensity as a sum over Eulerian peak positions, which are in turn related to their respective Lagrangian proto-halo positions

$$1+\delta_{\rm pk}(r) = \frac{1}{\bar{n}_{\rm pk}}\sum_{\rm pk}\delta_{\rm D}\left(r-r_{\rm pk}\right) = \int {\rm d}q'\delta_{\rm D}\left[r-q'-D_+\Psi(q')\right]\sum_{\rm pk}\delta_{\rm D}(q'-q_{\rm pk}), \tag{43}$$

$$= \frac{\sigma_2}{\sigma_1}\int {\rm d}q'\int\frac{{\rm d}k}{2\pi}\exp\left[\imath k(r-q')\right]|x_{11}(q')|\delta_{\rm D}[x_1(q')]\Theta_{\rm H}[-x_{11}(q')]\exp\left[-\imath k D_+\Psi(q')\right], \tag{44}$$

where we expanded the Dirac function as plane waves. The correlation of evolved peaks is therefore given by

$$\xi(r) = \langle\delta_{\rm pk}(0)\delta_{\rm pk}(r)\rangle = \frac{1}{\bar{n}_{\rm pk}^2}\frac{\sigma_2^2}{\sigma_1^2}\int {\rm d}Q\int\frac{{\rm d}k}{2\pi}\exp\left[\imath k(Q-r)\right]\langle\exp\left[-\imath k D_+(\Psi_1-\Psi_2)\right]$$
$$\times|x_{11}(q_1)||y_{11}(q_2)|\delta_{\rm D}[x_1(q_1)]\delta_{\rm D}[y_1(q_2)]\Theta_{\rm H}[-x_{11}(q_1)]\Theta_{\rm H}[-y_{11}(q_2)]\rangle - 1, \tag{45}$$

where $Q = q_2 - q_1$ is the Lagrangian separation of the peaks and Ψ_1 and Ψ_2 are the displacements at the respective positions. The displacement field is an additional stochastic variable that needs to be averaged over under the peak constraint. For this purpose, we need to append the covariance matrix by components that describe the auto-covariance of the displacement and the cross-covariance between the displacement on the one hand and the density field and its derivatives on the other hand. Splitting the state vector into $\boldsymbol{\Phi} = (\boldsymbol{X}, \boldsymbol{\Psi})$ where in this section we redefine $\boldsymbol{X}$ as $\boldsymbol{X} = (\sigma_0 x, 0, \sigma_2 x_{11}, \sigma_0 y, 0, \sigma_2 y_{11})$ and $\boldsymbol{\Psi} = (\Psi_1, \Psi_2)$, the covariance matrix (see Appendix B for an explicit expression) takes the following schematic form

$$\boldsymbol{C} = \begin{pmatrix}\langle\boldsymbol{X}\cdot\boldsymbol{X}^{\rm T}\rangle & \langle\boldsymbol{X}\cdot\boldsymbol{\Psi}^{\rm T}\rangle\\ \langle\boldsymbol{\Psi}\cdot\boldsymbol{X}^{\rm T}\rangle & \langle\boldsymbol{\Psi}\cdot\boldsymbol{\Psi}^{\rm T}\rangle\end{pmatrix} = \begin{pmatrix}\boldsymbol{C}_X & \boldsymbol{C}_{X\Psi}\\ \boldsymbol{C}_{X\Psi}^{\rm T} & \boldsymbol{C}_\Psi\end{pmatrix} = \begin{pmatrix}\boldsymbol{\Omega}_X & \boldsymbol{\Omega}_{X\Psi}\\ \boldsymbol{\Omega}_{X\Psi}^{\rm T} & \boldsymbol{\Omega}_\Psi\end{pmatrix}^{-1} = \boldsymbol{\Omega}^{-1}, \tag{46}$$

where $\boldsymbol{\Omega} = \boldsymbol{C}^{-1}$ is the precision matrix. The determinant of the covariance matrix can be decomposed into $\det\boldsymbol{C} = \det\boldsymbol{C}_X/\det\boldsymbol{\Omega}_\Psi$ with $\boldsymbol{\Omega}_\Psi = (\boldsymbol{C}_\Psi - \boldsymbol{C}_{X\Psi}^{\rm T}\cdot\boldsymbol{C}_X^{-1}\cdot\boldsymbol{C}_{X\Psi})^{-1}$, which will prove useful in the rest of the calculation. Defining $\imath k(\Psi_1-\Psi_2) = \imath k\,\boldsymbol{u}^{\rm T}\cdot\boldsymbol{\Psi}$ with $\boldsymbol{u} = (1,-1)$, one can rewrite the argument of the exponential arising from the PDF and the shift as

$$\boldsymbol{\Phi}^{\rm T}\cdot\boldsymbol{C}^{-1}\cdot\boldsymbol{\Phi} + 2\imath k D_+\,\boldsymbol{u}^{\rm T}\cdot\boldsymbol{\Psi} = \boldsymbol{X}^{\rm T}\cdot\boldsymbol{\Omega}_X\cdot\boldsymbol{X} + 2\boldsymbol{X}^{\rm T}\cdot\boldsymbol{\Omega}_{X\Psi}\cdot\boldsymbol{\Psi} + \boldsymbol{\Psi}^{\rm T}\cdot\boldsymbol{\Omega}_\Psi\cdot\boldsymbol{\Psi} + 2\imath D_+\,k\,\boldsymbol{u}^{\rm T}\cdot\boldsymbol{\Psi}$$
$$= \boldsymbol{X}^{\rm T}\cdot\boldsymbol{\Omega}_X\cdot\boldsymbol{X} + 2\boldsymbol{X}^{\rm T}\cdot\boldsymbol{\Omega}_{X\Psi}\cdot\boldsymbol{\Psi} + 2\boldsymbol{\mu}^{\rm T}\cdot\boldsymbol{\Omega}_\Psi\cdot\boldsymbol{\Psi} + 2\imath D_+\,k\,\boldsymbol{u}^{\rm T}\cdot\boldsymbol{\Psi} - \boldsymbol{\mu}^{\rm T}\cdot\boldsymbol{\Omega}_\Psi\cdot\boldsymbol{\mu} + (\boldsymbol{\Psi}-\boldsymbol{\mu})^{\rm T}\cdot\boldsymbol{\Omega}_\Psi\cdot(\boldsymbol{\Psi}-\boldsymbol{\mu}), \tag{47}$$

for any vector $\boldsymbol{\mu}$. Let us now complete the square to isolate the displacement part of the PDF and therefore choose $\boldsymbol{\mu}^{\rm T} = -(\boldsymbol{X}^{\rm T}\cdot\boldsymbol{\Omega}_{X\Psi} + \imath D_+\,k\,\boldsymbol{u}^{\rm T})\cdot\boldsymbol{\Omega}_\Psi^{-1}$. In that case, we get

$$\boldsymbol{\Phi}^{\rm T}\cdot\boldsymbol{C}^{-1}\cdot\boldsymbol{\Phi} + 2\imath k D_+\,\boldsymbol{u}^{\rm T}\cdot\boldsymbol{\Psi} = \boldsymbol{X}^{\rm T}\cdot\boldsymbol{C}_X^{-1}\cdot\boldsymbol{X} + D_+^2k^2\,\boldsymbol{u}^{\rm T}\cdot\boldsymbol{\Omega}_\Psi^{-1}\cdot\boldsymbol{u} + 2\imath D_+ k\boldsymbol{X}^{\rm T}\cdot\boldsymbol{C}_X^{-1}\cdot\boldsymbol{C}_{X\Psi}\cdot\boldsymbol{u} + (\boldsymbol{\Psi}-\boldsymbol{\mu})^{\rm T}\cdot\boldsymbol{\Omega}_\Psi\cdot(\boldsymbol{\Psi}-\boldsymbol{\mu}). \tag{48}$$

The displacement vector $\boldsymbol{\Psi}$ can be integrated out, yielding unity and leaves us with

$$\langle\delta_{\rm pk}(0)\delta_{\rm pk}(r)\rangle = \frac{1}{\bar{n}_{\rm pk}^2}\int {\rm d}Q\int\frac{{\rm d}k}{2\pi}\int {\rm d}\boldsymbol{X}\exp\left[\imath k(Q-r)\right]$$
$$\frac{w(\boldsymbol{X})}{\sqrt{(2\pi)^6\det\boldsymbol{C}_X}}\exp\left[-\frac{1}{2}\boldsymbol{X}^{\rm T}\cdot\boldsymbol{C}_X^{-1}\cdot\boldsymbol{X} - \frac{1}{2}D_+^2k^2\,\boldsymbol{u}^{\rm T}\cdot\boldsymbol{\Omega}_\Psi^{-1}\cdot\boldsymbol{u} - \imath D_+\,k\boldsymbol{X}^{\rm T}\cdot\boldsymbol{C}_X^{-1}\cdot\boldsymbol{C}_{X\Psi}\cdot\boldsymbol{u}\right] - 1, \tag{49}$$

where the joint peak condition is defined as

$$w(\boldsymbol{X}) = |x_{11}(q_1)||y_{11}(q_2)|\delta_{\rm D}[x_1(q_1)]\delta_{\rm D}[y_1(q_2)]\Theta_{\rm H}[-x_{11}(q_1)]\Theta_{\rm H}[-y_{11}(q_2)]. \tag{50}$$

Let us try to understand the linearized version of this result. Fourier transforming in the Eulerian separation r and expanding this expression for small correlations (i.e. $Q\to\infty$), we get to first order

$$P_{\rm pk}(k) = \frac{1}{\bar{n}_{\rm pk}^2}\int {\rm d}Q\int {\rm d}\boldsymbol{X}w(\boldsymbol{X})\left(-\frac{1}{2}\boldsymbol{X}^{\rm T}\cdot\boldsymbol{C}_X^{-1}\cdot\boldsymbol{X} - \frac{1}{2}D_+^2k^2\,\boldsymbol{u}^{\rm T}\cdot\boldsymbol{\Omega}_\Psi^{-1}\cdot\boldsymbol{u} - \imath D_+\,k\boldsymbol{X}^{\rm T}\cdot\boldsymbol{C}_X^{-1}\cdot\boldsymbol{C}_{X\Psi}\cdot\boldsymbol{u}\right)_{\mathcal{O}(\xi^1)}$$
$$\times\exp\left[\imath kQ\right]\exp\left[-D_+^2k^2\sigma_{v,{\rm pk}}^2\right]\exp\left[-\frac{1}{2}\frac{(x_{11}+\gamma x)^2}{1-\gamma^2} - \frac{1}{2}x^2\right]\exp\left[-\frac{1}{2}\frac{(y_{11}+\gamma y)^2}{1-\gamma^2} - \frac{1}{2}y^2\right]. \tag{51}$$

The expansions up to first order in correlations of the three constituent terms of the exponent are given by

$$-\frac{1}{2}\left(\boldsymbol{X}^{\mathrm{T}}\cdot\boldsymbol{C}_X^{-1}\cdot\boldsymbol{X}\right)_{\mathcal{O}(\xi^1)} = H_{10}(x,-x_{11})H_{10}(y,-y_{11})\frac{\xi_0}{\sigma_0^2} + H_{01}(x,-x_{11})H_{01}(y,-y_{11})\frac{\xi_2}{\sigma_2^2} + \left[H_{10}(x,-x_{11})H_{01}(y,-y_{11}) + H_{10}(y,-y_{11})H_{01}(x,-x_{11})\right]\frac{\xi_1}{\sigma_0\sigma_2}, \tag{52}$$

$$-\frac{1}{2}\left(\boldsymbol{u}^{\mathrm{T}}\cdot\boldsymbol{\Omega}_\Psi^{-1}\cdot\boldsymbol{u}\right)_{\mathcal{O}(\xi^1)} = \xi_{-1} - 2\xi_0\frac{\sigma_0^2}{\sigma_1^2} + \xi_1\frac{\sigma_0^4}{\sigma_1^4}, \tag{53}$$

$$\left(\boldsymbol{X}^{\mathrm{T}}\cdot\boldsymbol{C}_X^{-1}\cdot\boldsymbol{C}_{X\Psi}\cdot\boldsymbol{u}\right)_{\mathcal{O}(\xi^1)} = \frac{1}{\sigma_0}\left[H_{10}(x,-x_{11}) + H_{10}(y,-y_{11})\right]\left(\xi_{-1/2} - \frac{\sigma_0^2}{\sigma_1^2}\xi_{1/2}\right) + \frac{1}{\sigma_2}\left[H_{01}(x,-x_{11}) + H_{01}(y,-y_{11})\right]\left(\xi_{1/2} - \frac{\sigma_0^2}{\sigma_1^2}\xi_{3/2}\right), \tag{54}$$

where H_{ij} is defined in Section 4 and the peak velocity/displacement dispersion is given by

$$\sigma^2_{\mathrm{v,pk}} = \sigma^2_{-1} - \frac{\sigma_0^4}{\sigma_1^2}. \tag{55}$$

Note that the correlation functions ξ_i are defined in equation (38) and the σ_i in equation (15). Performing the integration over Q amounts to Fourier transforming the correlation functions in the above expressions. Performing this Fourier transform and averaging over the peak curvature variables x_{11} and y_{11}, we have

$$P_{\mathrm{pk}}(k) \approx \left[b_{10}(\nu_1) + b_{01}(\nu_1)k^2 + D_+\left(1 - \frac{\sigma_0^2}{\sigma_1^2}k^2\right)\right]\left[b_{10}(\nu_2) + b_{01}(\nu_2)k^2 + D_+\left(1 - \frac{\sigma_0^2}{\sigma_1^2}k^2\right)\right]P_{\mathrm{s}}(k)\exp\left[-D_+^2\,k^2\sigma^2_{\mathrm{v,pk}}\right]. \tag{56}$$

The propagator term $\exp\left[-D_+^2\,k^2\sigma^2_{\mathrm{v,pk}}\right]$ arising here is an artefact of our naïve expansion, its long wavelength contributions should cancel for equal-time correlators. Furthermore, the above expression does not contain the constant stochasticity corrections that are arising from small-scale effects – e.g exclusion – in the correlation function, where $\xi_i \approx \sigma_i^2$ and the above expansion fails.

At low wavenumbers and defining again $b \equiv b_{10}$, the peak density power spectrum simplifies to

$$P_{\mathrm{pk}}(k) \approx [b(\nu_1) + D_+][b(\nu_2) + D_+]P_{\mathrm{s}}(k), \tag{57}$$

meaning that the large-scale bias is given by $b + D_+$ as one would have expected from Mo & White (1996). In general however, the linear Lagrangian peak bias $b_{10} + b_{01}k^2$ decays to the velocity bias $1 - \sigma_0^2/\sigma_1^2k^2$ as discussed thoroughly in Desjacques & Sheth (2010), Desjacques et al. (2010) and Baldauf, Desjacques & Seljak (2015). In configuration space, this statistical velocity bias appears as $\psi_{\mathrm{pk}} = \psi - \sigma_0^2/\sigma_1 x_1$ (Desjacques 2008).

Having shown the consistency with previous 3D studies, let us come back to the full expression given by equation (49). Together with the prefactor $\exp[\imath k(r-Q)]$, this is a Gaussian integral in k, which is readily performed and yields

$$\langle\delta_{\mathrm{pk}}(0)\delta_{\mathrm{pk}}(r)\rangle = \int \mathrm{d}Q\; F(Q|r) - 1, \tag{58}$$

where

$$F(Q|r) = \frac{1}{\bar{n}_{\mathrm{pk}}^2}\int \mathrm{d}\boldsymbol{X}\,\frac{w(\boldsymbol{X})}{\sqrt{(2\pi)^6\det\boldsymbol{C}_X}}\exp\left[-\frac{1}{2}\boldsymbol{X}^{\mathrm{T}}\cdot\boldsymbol{C}_X^{-1}\cdot\boldsymbol{X}\right]\frac{1}{\sqrt{2\pi D_+^2\,\boldsymbol{u}^{\mathrm{T}}\cdot\boldsymbol{\Omega}_\Psi^{-1}\cdot\boldsymbol{u}}}\exp\left[-\frac{1}{2}\frac{(Q - r - D_+\boldsymbol{X}^{\mathrm{T}}\cdot\boldsymbol{C}_X^{-1}\cdot\boldsymbol{C}_{X\Psi}\cdot\boldsymbol{u})^2}{D_+^2\,\boldsymbol{u}^{\mathrm{T}}\cdot\boldsymbol{\Omega}_\Psi^{-1}\cdot\boldsymbol{u}}\right], \tag{59}$$

which is a convolution between the Eulerian and Lagrangian distances r and Q. For a fixed Eulerian distance, the integral is approximately Gaussian and peaks at $Q_{\mathrm{p}} = r + D_+\boldsymbol{X}^{\mathrm{T}}\cdot\boldsymbol{C}_X^{-1}\cdot\boldsymbol{C}_{X\Psi}\cdot\boldsymbol{u}$ (as illustrated in Fig. 6). As the growth factor D_+ goes to zero, the last part of the above integral becomes a Dirac delta function for $Q - r$ and we recover the Lagrangian expression. The shift term $D_+\boldsymbol{X}^{\mathrm{T}}\cdot\boldsymbol{C}_X^{-1}\cdot\boldsymbol{C}_{X\Psi}\cdot\boldsymbol{u}$ corresponds by construction to the most likely difference of Zel'dovich displacements, $\boldsymbol{\Psi}^{\mathrm{T}}\cdot\boldsymbol{u}$, (in the Wiener filtering sense) for a given $\boldsymbol{X}$; it is negligible on large scales, but can lead to significant corrections on small scales so that the convolution by these conditional displacements actually fill the $\xi = -1$ region.

In order to compute the effect of the peak displacements, we have to resort to 1D power spectra that grow steeper than k^1 for low wavenumbers since otherwise the velocity correlators diverge in the infrared (k^{n-2} is not integrable). In particular, we need a power spectrum that has a slope $n > 1$ and we will choose $n = 3$ for definiteness. We show the evolved correlation function and bias in Fig. 7. Non-linearities tend to wash out the exclusion and decrease the small-scale clustering of peaks.

In Baldauf et al. (2013), it has been shown in simulations that the stochasticity amplitude on large scales is the same in Lagrangian and Eulerian space. On small scales, the corrections to the fiducial $1/\bar{n}$ stochasticity have to vanish, and they do so for haloes in Eulerian and proto-haloes in Lagrangian space. The only change in the behaviour is that the transition happens at higher wavenumbers in Eulerian space.

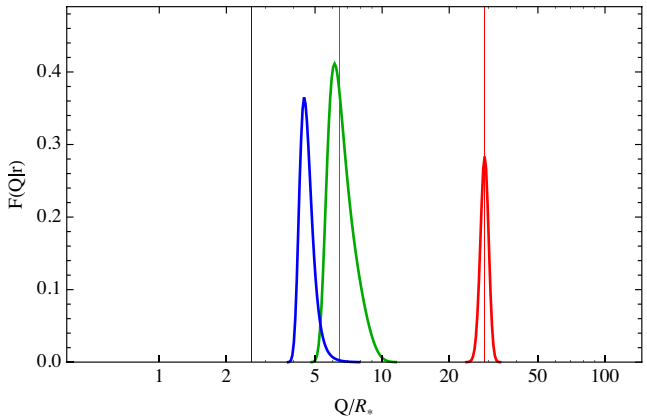

Figure 6. Contribution to the integral over Lagrangian separations in equation (58) for $D_+ = 7$. The vertical lines indicate the Eulerian separation r and the corresponding curves indicate the support of the integral. We see that for large scales, the evolution merely corresponds to a convolution with a Gaussian, whereas for small scales there is a an offset in the support to larger scales and the convolution kernel is skewed.

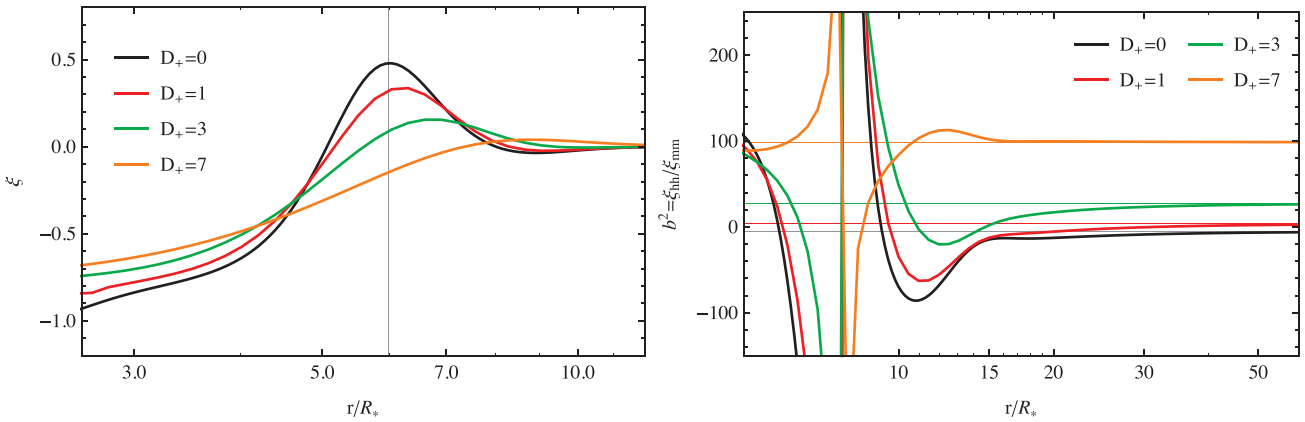

Figure 7. Left-hand panel: small-scale correlation function of initial and evolved peaks in a $n = 3$ power-law density field. We have chosen peaks of height $\bar{\nu} = 6/5$ and $\Delta\nu = 3/5$ to highlight the behaviour in presence of exclusion. The linear growth factor increases from the initial conditions $D_+ = 0$ to some arbitrary final time $D_+ = 7$. Right-hand panel: linear bias of the peak correlation functions with respect to the linear matter correlation function. We clearly see that the bias asymptotes to the expected $b_{10} + D_+$ behaviour for large separations indicated by the horizontal lines.

We would like to explore to what extend our 1D peak model can reproduce this behaviour. In Fig. 8, we show the power spectrum of peaks in Lagrangian space and their stochasticity estimated as $P_{\rm pk} - b^2 P_{\rm s}$. We see that the large-scale amplitude is the same for initial and evolved haloes in agreement with numerical studies. After correction for the large-scale bias in Eulerian space, we also recover that the transition between the non-zero and zero stochasticity correction regimes is pushed to higher wavenumbers.

5.2 Streaming motions of peaks

The mean motion of peaks can be understood based on their initial velocity statistics. The displacement in the Zel'dovich approximation is just the time integral of the velocity. In the previous section, we assumed that the peaks move according to their initial velocities, where $\boldsymbol{\Psi} = \boldsymbol{v}/\mathcal{H}f$. Using this relation between displacements and velocities, we will continue working with displacements but note that our results are related to velocity statistics by a simple time dependent but scale-independent prefactor. Let us for this purpose consider the mean infall $v_{12}/\mathcal{H}f = \left\langle (\Psi_2 - \Psi_1)(1+\delta_{\rm pk,1})(1+\delta_{\rm pk,2})\right\rangle / (1+\xi_{\rm pk})$, where $\Psi_i = v_i/\mathcal{H}f$ and $\delta_{{\rm pk},i}$ are the displacements and peak densities at positions 1 and 2, respectively. This mean streaming is an important ingredient for redshift space distortion models [see e.g. Reid & White (2011)]. In a fashion similar to what was presented above for displaced peaks but taking $D_+ = 0$, we have

$$(1+\xi_{\rm pk})\frac{v_{12}}{\mathcal{H}f} = \frac{\left\langle (v_2 - v_1)(1+\delta_{\rm pk,1})(1+\delta_{\rm pk,2})\right\rangle}{\mathcal{H}f} = -\frac{1}{\bar{n}_{\rm pk}^2}\int {\rm d}\boldsymbol{X}\; \boldsymbol{X}^{\rm T}\cdot\boldsymbol{C}_X^{-1}\cdot\boldsymbol{C}_{X\Psi}\cdot\boldsymbol{u}\;\frac{w(\boldsymbol{X})}{\sqrt{(2\pi)^6\det\boldsymbol{C}_X}}\exp\left[-\frac{1}{2}\boldsymbol{X}^{\rm T}\cdot\boldsymbol{C}_X^{-1}\cdot\boldsymbol{X}\right]\,. \tag{60}$$

On large scales, this quantity can be approximated by its linear (scale-dependent) bias expansion

$$\frac{v_{12}}{\mathcal{H}f} \approx -\left[2b_{10}\left(\xi_{-1/2} - \frac{\sigma_0^2}{\sigma_1^2}\xi_{1/2}\right) + 2b_{01}\left(\xi_{1/2} - \frac{\sigma_0^2}{\sigma_1^2}\xi_{3/2}\right)\right]\frac{Q}{|Q|}\,, \tag{61}$$

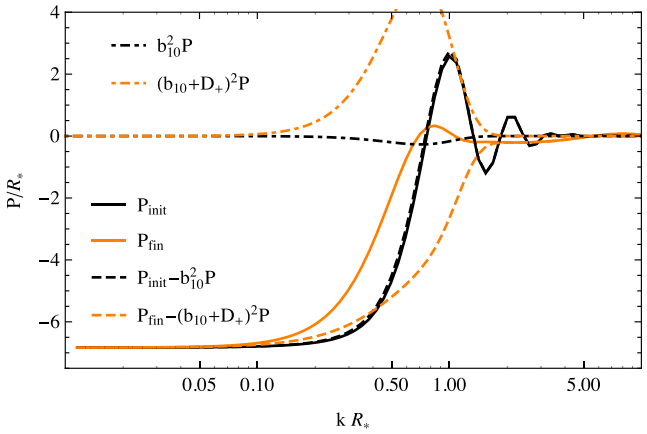

Figure 8. Evolution of the peak–peak power spectrum and its noise component $P_{\rm pk} - b^2 P_{\rm s}$ from the initial conditions to the final configuration at $D_+ = 7$. While the amplitude of the stochasticity correction remains constant on large scales, the infall causes the transition to zero to happen on smaller scales/larger wavenumbers.

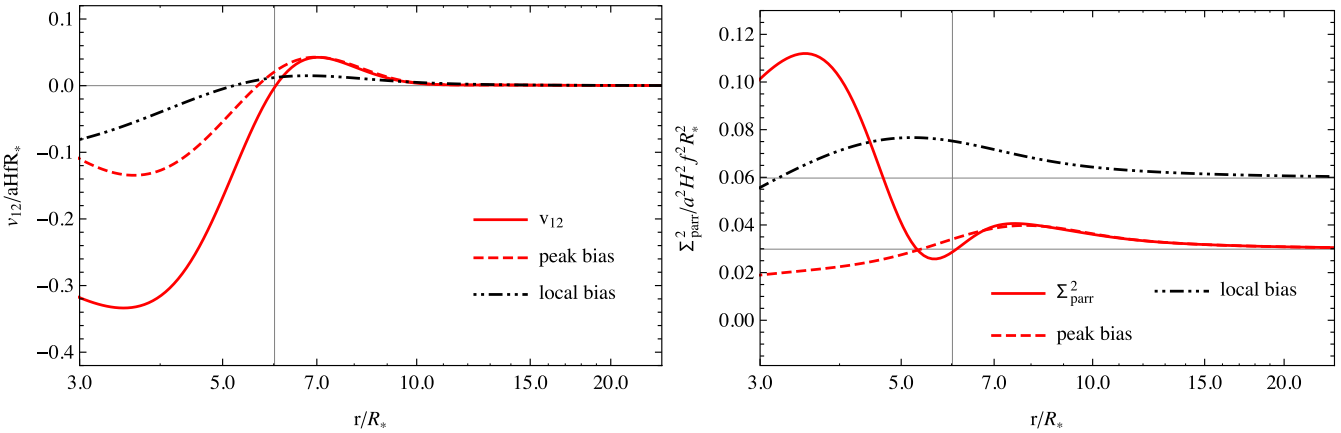

Figure 9. Left-hand panel: mean relative velocity v_{12} of 1D peaks (red solid). The peak velocities clearly deviate from the velocities of random dark matter particles (black dot–dashed) on small scales. On large scales, this deviation can be described by a linear velocity bias (red dashed), which however fails to describe the non-perturbative behaviour in the exclusion regime. We see that below $r = 6R_\star$, peaks are moving towards each other and away from each other for larger separations. The vertical grey line indicates the peak of the correlation function in Fig. 7. Right-hand panel: velocity dispersion of the peaks in 1D. Even the large separation limit of the peak velocity dispersion deviates from the underlying dark matter, i.e. local bias (black dot–dashed), due to the correction in the peak displacement dispersion equation (55). This difference and the onset of the scale-dependence is described by the linear scale-dependent peak velocity dispersion bias (red dashed) in equation (63).

in agreement with 3D results (Desjacques & Sheth 2010). By contrast, the mean infall in the local bias model reads $v_{12} \approx -2b\xi_{-1/2}Q/|Q|$, where $\xi_{-1/2}$ is usually evaluated without an explicit smoothing scale. In Fig. 9, we show the mean relative velocity of the same sample of peaks considered for the evolution above, i.e. peaks of height $\bar{\nu} = 3/2$ and $\Delta\nu = 3/5$ in a $n = 3$ power-law density field. For the underlying matter distribution, we have $v_{12}/(\mathcal{H}f) \approx -2\xi_{-1/2}Q/|Q|$. We clearly see that matter and peak mean streaming differ for scales $r < 10R_\star$. This deviation is captured by the scale-dependent peak velocity bias equation (61) down to $r \approx 7R_\star$. Thus, the linear peak velocity bias starts to deviate at larger separations than the linear peak density bias. Note that the distance shown in this figure corresponds to the mean offset between the Eulerian separation and the Lagrangian separation in Fig. 6. Let us finish our considerations about the peak dynamics by considering the velocity dispersion, $(\sigma_{12}/\mathcal{H}f)^2 = \big\langle(\Psi_2 - \Psi_1)^2(1+\delta_{\rm pk,1})(1+\delta_{\rm pk,2})\big\rangle/(1+\xi_{\rm pk})$, which can be exactly calculated as

$$(1+\xi_{\rm pk})\frac{\sigma_{12}^2}{(\mathcal{H}f)^2} = \frac{1}{\bar{n}_{\rm pk}^2}\int {\rm d}\boldsymbol{X}\left[\left(\boldsymbol{X}^{\rm T}\cdot\boldsymbol{C}_X^{-1}\cdot\boldsymbol{C}_{X\Psi}\cdot\boldsymbol{u}\right)^2 + \boldsymbol{u}^{\rm T}\cdot\boldsymbol{\Omega}_\Psi^{-1}\cdot\boldsymbol{u}\right]\frac{w(\boldsymbol{X})}{\sqrt{(2\pi)^6\det\boldsymbol{C}_X}}\exp\left[-\frac{1}{2}\boldsymbol{X}^{\rm T}\cdot\boldsymbol{C}_X^{-1}\cdot\boldsymbol{X}\right]. \tag{62}$$

For large separations – or equivalently small correlation functions –, we get the following approximate expression

$$\frac{\sigma_{12}^2}{(\mathcal{H}f)^2} \approx 2\sigma_{v,\rm pk}^2 - 2\left(\xi_{-1} - 2\frac{\sigma_0^2}{\sigma_1^2}\xi_0 + \frac{\sigma_0^4}{\sigma_1^4}\xi_1\right). \tag{63}$$

This result could have been obtained using the peak density and velocity bias in

$$\sigma_{12}^2 \approx \left(\left\langle v_1^2\right\rangle + \left\langle v_2^2\right\rangle\right) - 2\left\langle v_1 v_2\right\rangle\ . \tag{64}$$

Equation (63) is to be compared with the expectation of the velocity dispersion in the local bias model which reads at leading order of $2\sigma^2_{-1} - 2\xi_{-1}$ evaluated without an explicit smoothing scale.

In this section, we have derived an expression for calculating the evolved peak correlation function on all scales, assuming that the peaks evolve according to the Zel'dovich approximation. We have seen that non-perturbative effects persist even for the evolved field, which is partially due to the peak effects in the mean relative displacement and displacement dispersion.

6 CONCLUSIONS

Halo exclusion is an essential ingredient towards a realistic description of the two-halo term, which encodes most of the cosmological information that can be extracted from the two-point correlation of biased tracers. Halo exclusion stems from the fact that one cannot find two peaks of the mass density field (haloes) arbitrary close to each other or even overlap. Until very recently however, this effect had been either completely ignored or crudely modelled by setting $\xi_{\rm h}(r) = -1$ at separations r less than the sum of the halo virial radii, while sticking to the linear bias approximation at larger distances.

In this paper, we have investigated this small-scale exclusion using a simple, well-motivated approximation: the clustering of Gaussian density peaks and, more general, critical points in one dimension. After studying the small-r behaviour for various power-law spectra and its sensitivity to the peak height, we have shown that the two-point correlation function of 1D density peaks differs significantly from the crude, aforementioned prescription. We have also explored how peak exclusion affects the convergence of the perturbative bias expansion in real and Fourier space. Finally, we have included the displacement from the initial to final peak position according to the Zel'dovich approximation to clarify how exclusion effects mix up with scale-dependences induced by the non-linear gravitational evolution.

Our key findings can be summarized in the following points.

(i) The correlation function of equal height peaks or critical points ($\Delta\nu = 0$) asymptotes to a finite non-zero number at small scales.

(ii) The correlation function of unequal height peaks or critical points ($\Delta\nu \neq 0$) deviates from the aforementioned case on small scales and asymptotes to exactly -1, where a percent deviation from $\Delta\nu = 0$ is typically reached for $r_{1\,\rm per\,cent} \approx (180\Delta\nu)^{1/3} R_\star$; this scale is valid for a broad range of power spectra including projected ΛCDM.

(iii) The local bias expansion fails to describe the scale-dependence starting at very large scales, the peak bias series including derivative operators fares better but its convergence in the $r \approx R_\star$ regime is very slow and it completely fails in the exclusion regime.

(iv) Time evolution enhances the large-scale clustering according to the well-known $b + D_+$ behaviour and leads to significant modifications in the exclusion regime where non-linearities reduce the small-scale clustering of peaks.

(v) The statistics of the relative displacement of peaks is within reach of the formalism and is shown to depart significantly from the mean streaming of the dark matter field, the validity of the peak bias expansion in this regime is reduced compared to the case of the density field.

Even though our findings apply, strictly speaking, to the clustering of tracers in 1D density fields, they provide useful insights into halo exclusion and its impact on the two-halo term in a realistic setting in three dimensions. It would certainly be interesting but computationally more challenging to study these effects for peaks in 3D density fields. This will be addressed in an upcoming paper.

ACKNOWLEDGEMENTS

We thank D. Pogosyan for useful comments during the course of this work. VD thanks the LABEX 'Institut de Lagrange de Paris' for funding and acknowledges support from the Swiss National Science Foundation. TB gratefully acknowledges support by the Institute for Advanced Study through the Corning Glass works foundation fund. CP and SC thank the University of Geneva for funding and the community of http://mathematica.stackexchange.com for technical advice. This research is part of the Spin(e) (ANR-13-BS05-0005, http://cosmicorigin.org) and the Cosmo@NLO grants of the French Agence Nationale de la Recherche.

REFERENCES

Baldauf T., Seljak U., Smith R. E., Hamaus N., Desjacques V., 2013, Phys. Rev. D, 88, 083507
Baldauf T., Desjacques V., Seljak U., 2015, Phys. Rev. D, 92, 123507
Bardeen J. M., Bond J. R., Kaiser N., Szalay A. S., 1986, ApJ, 304, 15
Beltrán Jiménez J., Durrer R., 2011, Phys. Rev. D, 83, 103509
Buchert T., 1989, A&A, 223, 9
Casas-Miranda R., Mo H. J., Sheth R. K., Boerner G., 2002, MNRAS, 333, 730
Coles P., 1989, MNRAS, 238, 319
Desjacques V., 2008, Phys. Rev. D, 78, 103503
Desjacques V., 2013, Phys. Rev. D, 87, 043505
Desjacques V., Sheth R. K., 2010, Phys. Rev. D, 81, 023526
Desjacques V., Crocce M., Scoccimarro R., Sheth R. K., 2010, Phys. Rev. D, 82, 103529
Gay C., Pichon C., Pogosyan D., 2012, Phys. Rev. D, 85, 023011
Hamaus N., Seljak U., Desjacques V., Smith R. E., Baldauf T., 2010, Phys. Rev. D, 82, 043515
Kac M., 1943, Bull. Am. Math. Soc., 49, 938
Lumsden S. L., Heavens A. F., Peacock J. A., 1989, MNRAS, 238, 293

McQuinn M., White M., 2015, preprint (arXiv:e-prints)
Manera M., Gaztañaga E., 2011, MNRAS, 415, 383
Mo H. J., White S. D. M., 1996, MNRAS, 282, 347
Pogosyan D., Pichon C., Gay C., Prunet S., Cardoso J. F., Sousbie T., Colombi S., 2009, MNRAS, 396, 635
Regos E., Szalay A. S., 1995, MNRAS, 272, 447
Reid B. A., White M., 2011, MNRAS, 417, 1913
Rice S. O., 1945, Bell Syst. Tech. J., 25, 46
Seljak U., Hamaus N., Desjacques V., 2009, Phys. Rev. Lett., 103, 091303
Sheth R. K., Lemson G., 1999, MNRAS, 304, 767
Smith R. E., Scoccimarro R., Sheth R. K., 2007, Phys. Rev. D, 75, 063512
Smith R. E., Desjacques V., Marian L., 2011, Phys. Rev. D, 83, 043526
Yoshisato A., Matsubara T., Morikawa M., 1998, ApJ, 498, 48

APPENDIX A: EXPLICIT EXPRESSION FOR SMALL RADII

At small radii, it has been shown in Section 3.2 that the signed critical point correlation function can be expanded at small separations

$$1+\xi_{\rm crit}\left(\tilde{r},\nu-\frac{\Delta\nu}{2},\nu+\frac{\Delta\nu}{2},n=0\right)=\frac{\sqrt{3}}{\left(\Delta\nu^2-4\nu^2\right)}\left[\alpha_8(\nu,\Delta\nu)\frac{\Delta\nu^2}{\tilde{r}^8}+\alpha_6(\nu,\Delta\nu)\frac{\Delta\nu^2}{\tilde{r}^6}+\alpha_4(\nu,\Delta\nu)\frac{\Delta\nu^2}{\tilde{r}^4}+\alpha_2(\nu,\Delta\nu)\frac{\Delta\nu^2}{5\tilde{r}^2}\right.$$
$$\left.+\alpha_0(\nu,\Delta\nu)\right]\exp\left[\frac{\nu^2}{4}+\frac{7\Delta\nu^2}{80}-\frac{9\Delta\nu^2}{5\tilde{r}^2}+\frac{27\Delta\nu^2}{\tilde{r}^4}-\frac{324\Delta\nu^2}{\tilde{r}^6}\right]+\mathcal{O}(\tilde{r}),\tag{A1}$$

where the polynomials $\alpha_{2n}(\nu,\Delta\nu)$ for n between 0 and 4 are given by

$$\alpha_0(\nu,\Delta\nu)=-\frac{3\nu^2+8}{6}+\frac{\Delta\nu^2\left(315\nu^8+1680\nu^6+6720\nu^4-121\,856\nu^2+280\,576\right)}{1720\,320}+\frac{\Delta\nu^4\left(3645\nu^6+5940\nu^4+55\,776\nu^2-409\,856\right)}{43\,008\,000}$$
$$+\frac{9\Delta\nu^6\left(32\,805\nu^4-16\,200\nu^2+258\,976\right)}{20\,070\,400\,000}+\frac{59\,049\Delta\nu^8\left(27\nu^2-28\right)}{1404\,928\,000\,000}+\frac{129\,140\,163\Delta\nu^{10}}{3933\,798\,400\,000\,000},$$

$$\alpha_2(\nu,\Delta\nu)=\frac{3\left(2048-320\nu^2-15\nu^6\right)}{1280}-\frac{3\Delta\nu^2\left(3645\nu^4-5760\nu^2+39\,232\right)}{896\,000}-\frac{2187\Delta\nu^4\left(81\nu^2-128\right)}{125\,440\,000}-\frac{4782\,969\Delta\nu^6}{87\,808\,000\,000},$$

$$\alpha_4(\nu,\Delta\nu)=\frac{9}{16}\left(9\nu^4-24\nu^2+128\right)+\frac{81\Delta\nu^2\left(81\nu^2-172\right)}{5600}+\frac{531\,441\Delta\nu^4}{7840\,000},$$

$$\alpha_6(\nu,\Delta\nu)=162\left(8-3\nu^2\right)-\frac{19\,683\Delta\nu^2}{350},$$

$$\alpha_8(\nu,\Delta\nu)=23\,328.$$

When $\Delta\nu>0$, the signed critical point correlation function tends to -1 at small separations and therefore shows a clear exclusion zone while for $\Delta\nu=0$, it tends to a constant different from -1 and given by

$$1+\xi_{\rm crit}\left(\tilde{r},\nu,\nu,n=0\right)=\sqrt{3}\left(\frac{1}{8}+\frac{1}{3\nu^2}\right)\exp\left[\frac{\nu^2}{4}\right]+\mathcal{O}(\tilde{r}).\tag{A2}$$

It has to be noted that this constant is negative only for ν roughly between 1 and 2 for $n=0$ power-law power spectra.

APPENDIX B: COVARIANCE MATRIX

The&& covariance matrice of $\boldsymbol{X}$ and $\boldsymbol{\Psi}$ defined in Section 5 are given by

$$\boldsymbol{C}_X=\begin{pmatrix}\sigma_0^2 & 0 & -\sigma_1^2 & \xi_0 & -\xi_{\frac{1}{2}} & -\xi_1\\ 0 & \sigma_1^2 & 0 & \xi_{\frac{1}{2}} & \xi_1 & -\xi_{\frac{3}{2}}\\ -\sigma_1^2 & 0 & \sigma_2^2 & -\xi_1 & \xi_{\frac{3}{2}} & \xi_2\\ \xi_0 & \xi_{\frac{1}{2}} & -\xi_1 & \sigma_0^2 & 0 & -\sigma_1^2\\ -\xi_{\frac{1}{2}} & \xi_1 & \xi_{\frac{3}{2}} & 0 & \sigma_1^2 & 0\\ -\xi_1 & -\xi_{\frac{3}{2}} & \xi_2 & -\sigma_1^2 & 0 & \sigma_2^2\end{pmatrix},\tag{B1}$$

$$\boldsymbol{C}_{X\Psi}^{\mathrm{T}} = \begin{pmatrix} 0 & \sigma_0^2 & 0 & \xi_{-\frac{1}{2}} & \xi_0 & -\xi_{\frac{1}{2}} \\ -\xi_{-\frac{1}{2}} & \xi_0 & \xi_{\frac{1}{2}} & 0 & \sigma_0^2 & 0 \end{pmatrix}, \quad \text{and} \quad \boldsymbol{C}_{\Psi} = \begin{pmatrix} \sigma_{-1}^2 & \xi_{-1} \\ \xi_{-1} & \sigma_{-1}^2 \end{pmatrix}. \tag{B2}$$

This paper has been typeset from a TEX/LATEX file prepared by the author.